
Removing the fat from your posterior samples with MARGARINE

Harry T. J. Bevins^{*,1} William J. Handley^{1,2} Pablo Lemos^{3,4} Peter H. Sims⁵

Eloy de Lera Acedo^{1,2}

Anastasia Fialkov^{2,3}

Justin Alsing⁷

¹ Astrophysics Group, Cavendish Laboratory, Cambridge, CB3 0HE, UK

² Kavli Institute for Cosmology, Cambridge, CB3 0HA, UK

³ Department of Physics & Astronomy, University College London, London, WC1E 6BT, UK

⁴ Department of Physics and Astronomy, University of Sussex, Brighton, BN1 9QH, UK

⁵ Department of Physics and McGill Space Institute, McGill University,
Montreal, QC H3A 2T8, Canada

⁶ Institute of Astronomy, University of Cambridge, Cambridge CB3 0HA, UK

⁷ Oskar Klein Centre for Cosmoparticle Physics, Department of Physics,
Stockholm University, Stockholm SE-106 91, Sweden

*htjb2@cam.ac.uk

Abstract

Bayesian workflows often require the introduction of nuisance parameters, yet for core science modelling one needs access to a marginal posterior density. In this work, we use masked autoregressive flows and kernel density estimators to encapsulate the marginal posterior, allowing us to compute marginal Kullback–Leibler divergences and marginal Bayesian model dimensionalities in addition to generating samples and computing marginal log probabilities. We demonstrate this in application to topical cosmological examples of the Dark Energy Survey, and global 21-cm signal experiments. In addition to the computation of marginal Bayesian statistics, this work is important for further applications in Bayesian experimental design, complex prior modelling and likelihood emulation. This technique is made publicly available in the pip-installable code MARGARINE.

1 Introduction

Bayesian analysis is a cornerstone of modern statistical inference, and the Kullback-Leibler divergence [1] and Bayesian dimensionality [2] are important summary statistics for describing the complexity of the fit and the effective number of parameters being fitted. Bayesian analysis uses Bayes theorem to iteratively update the probability of a given hypothesis or model (posterior) given existing knowledge about the model parameters (prior) and a representative probability distribution for the data given the choice of model and parameters at each iteration (likelihood).

The technique has been applied in the inference of cosmological parameters from experiments such as the CMB mapper Planck [3], the Dark Energy Survey (DES, [4, 5, 6]), 21-cm power spectrum experiments (such as HERA [7], LOFAR [8, 9] and MWA [10, 11]) and global or sky-averaged 21-cm experiments (such as REACH [12]).

These experiments are often plagued by ‘nuisance’ parameters that characterise foregrounds and instrumental effects in the data. This leads to high dimensional parameter spaces, of which only a few of the parameters model the signal. Consequently, drawing conclusions about the parameters of interest and making model comparisons can be challenging. For example, in the Year 1 DES analysis the likelihood contains a total of 26 parameters of which 20 could be considered nuisance parameters with only 6 corresponding to cosmological parameters of interest [4]. Similarly, the REACH likelihood can contain upwards of 15 parameters, with only 3-7 of these corresponding to the global or sky-averaged 21-cm signal.

We present a means by which to numerically calculate *marginal* Kullback-Leibler divergences and Bayesian dimensionalities using Masked Autoregressive Flows (MAFs, [13]) and Kernel Density Estimators (KDEs, [14, 15]) to effectively learn and sample posterior distributions of signal subspaces in high dimensional data models. This allows us to determine the properties of cosmological subspaces, such as their log-probability densities and how well constrained they are, independent of the nuisance parameters in our analysis. We implement our approach in PYTHON and release the code as the pip installable package MARGARINE. The code is fully documented with worked examples, subject to continuous integration testing and does not require high performance computing to be used. This tool is invaluable to the Bayesian workflow and allows for direct and specific comparison of the constraining ability of different experimental approaches, which can in turn lead to improvements in experimental design.

In section 2 we outline in more detail the theory of Bayesian analysis, the statistical quantities that MARGARINE can estimate and the motivation behind the development of MARGARINE. We discuss the two different types of density estimators used by MARGARINE in section 3. In section 4, we apply MARGARINE to toy example posteriors and demonstrate that we can recover estimates of the KL divergence and Bayesian dimensionality accurately. We then demonstrate the application of the software to real world examples, including samples from DES and an example set of samples from the REACH pipeline. In section 5, we summarise our results.

2 Theory

2.1 Bayesian analysis and Bayesian evidence

Bayesian analysis is concerned with the estimation of posterior probabilities using Bayes theorem

$$P(\theta|D, M) = \frac{P(D|\theta, M)P(\theta|M)}{P(D|M)} = \frac{\mathcal{L}(\theta)\pi(\theta)}{\mathcal{Z}}, \quad (1)$$

where θ are the parameters of our model M describing the data D and $\mathcal{L}(\theta)$ corresponds to the likelihood. The prior, $\pi(\theta) = P(\theta|M)$, encodes our existing knowledge about the parameters before any sampling is performed. $\pi(\theta)$ is often chosen to be uniform or log-uniform for each parameter.

The evidence, \mathcal{Z} , is a marginal likelihood integrated over all the parameters and weighted by the prior

$$\mathcal{Z} = \int \mathcal{L}(\theta)\pi(\theta)d\theta. \quad (2)$$

The estimation of \mathcal{Z} via equation (2) is the primary concern of the nested sampling algorithm [16]. However, by equation (1) this calculation also returns samples on the posterior which can then be used to determine typical values of θ given the data.

2.2 KL divergence

The KL divergence is typically used as a loss function when training neural networks, however, it can be used to quantify the contraction from prior to posterior in a Bayesian analysis giving a measure of the constraining power of a model or experiment. It is defined as the average Shannon Information

$$\mathcal{I}(\theta) = \log \left(\frac{\mathcal{P}(\theta)}{\pi(\theta)} \right) \quad (3)$$

over the posterior, $\mathcal{P}(\theta)$,

$$\mathcal{D}(\mathcal{P}||\pi) = \int \mathcal{P}(\theta) \log \left(\frac{\mathcal{P}(\theta)}{\pi(\theta)} \right) d\theta = \langle \mathcal{I} \rangle_{\mathcal{P}} \approx \log \frac{V_{\pi}}{V_{\mathcal{P}}}, \quad (4)$$

and is a measure of how much information the data provides us about the parameter space. It is approximately equal to the log of the ratio of the prior volume, V_{π} , and the posterior volume, $V_{\mathcal{P}}$. \mathcal{D} is a strong function of the prior, and inherits the property of being additive for independent parameters from the Shannon Information. Calculation of the KL divergence requires the posterior distribution to be appropriately normalised and consequently the quantity is not attainable with common MCMC sampling techniques and more computationally intensive algorithms such as nested sampling have to be implemented to attain the Bayesian evidence.

A higher KL divergence indicates a larger information gain when moving from the prior to the posterior. This information gain is not always visible in the traditionally used corner plots showing 1D and 2D marginal posteriors, and consequently the KL divergence is a useful measure of the constraining power of the data [2].

The KL divergence can be shown to be invariant under a change of variables, meaning that its value in complex hard to learn spaces can be calculated in simpler transformed spaces (see section 3).

2.3 Bayesian Model Dimensionality

An alternative measure of constraint is the Bayesian Model Dimensionality [2] which gives a measure of the effective number of parameters that are being constrained and can be used to quantify tensions between different experimental results [17, 18]. The BMD d is given by

$$\frac{d}{2} = \int \mathcal{P}(\theta) \left(\log \left(\frac{\mathcal{P}(\theta)}{\pi(\theta)} \right) - \mathcal{D} \right) d\theta = \text{var}(\mathcal{I})_{\mathcal{P}} = (\langle (\log \mathcal{L})^2 \rangle_{\mathcal{P}} - \langle \log \mathcal{L} \rangle_{\mathcal{P}}^2), \quad (5)$$

and a full derivation can be found in [2]. The quantity is the variance of the Shannon information and therefore a higher order statistic than the KL divergence. It is only weakly prior dependent and like the KL divergence is additive for independent parameters and invariant under a change of variables.

2.4 Motivation

The goal of this paper is to demonstrate the use of masked autoregressive flows and Kernel Density Estimators in the calculation of marginal Bayesian statistics.

If our model $M(\theta)$ contains nuisance parameters and cosmological signal, then we can write $\theta = \{\theta_{\text{N}}, \theta_{\text{sig}}\}$. Mathematically, the marginal posterior for the signal parameters can be calculated by integrating out the dependence on θ_{N} .

However, $\mathcal{P}(\theta_{\text{sig}})$ is typically a difficult quantity to calculate. By using different density estimators to effectively perform this marginalisation and learn the signal subspace, we can not only sample specifically $\mathcal{P}(\theta_{\text{sig}})$ but also empirically calculate $\log(\mathcal{P}(\theta_{\text{sig}}))$. In turn, this allows us to calculate the marginal Bayesian statistics, which are the focus of this paper.

For example, the marginal KL divergence tells you how much information is gained by contracting specifically the signal prior onto the signal posterior without including contributions from correlations with or constraints on the nuisance foreground and systematic parameters. This allows us to confidently compare the information gained from different data sets from different experiments measuring the same signal, regardless of their specific foreground and/or systematic modelling. Similarly, the marginal BMD can be used to compare the effective number of *signal* parameters constrained by different experiments and models.

Using density estimators to calculate the KL divergence, marginal or not, also has the added advantage that it does not require knowledge of the Bayesian evidence provided the choice of density estimator returns a normalized probability distribution.

Further, since the density estimators are used to empirically approximate the logarithm of any posterior distribution, then the density estimator can be used as a computationally inexpensive likelihood generator [19].

Finally, we note that if the density estimator is set up correctly such that it is a bijective transformation between the unit hyper-cube and the target posterior then it can be used to generate samples from a sub-set, say cosmological, or the whole of one posterior as a prior on a subsequent nested sampling run. This allows you to use far more complex priors and to provide a more realistic summary of the current knowledge of the parameter space to the Bayesian inference [20].

3 Density Estimators in Practice

In principle, you can use any type of density estimator to model subspaces in a larger parameter space and calculate the marginal Bayesian statistics discussed. The only requirements are that it can be used to resample the space and approximate the normalised log-probability associated with the posterior subspace.

3.1 Masked Autoregressive Flows

Complex bijectors can be built using neural networks to transform from one multivariate distribution to another. We start with a base distribution, a multivariate standard normal distribution, $z_0 \sim \mathcal{N}(0, 1)$ which is then repeatedly shifted and scaled so that the KL divergence between the target and bijector output is minimised in an iterative processes

$$\begin{aligned} z_0 &= \mathcal{N}(0, 1) \\ z_1 &= z_0\sigma_1(z_0, w) + \mu_1(z_0, w) \\ &\vdots \\ x &= z_{n-1}\sigma_n(z_{n-1}, w) + \mu_n(z_{n-1}, w) \end{aligned} \tag{6}$$

The shifting and scaling parameters, μ_i and σ_i , are determined by the outputs and weights, w , of autoregressive neural networks and are conditional on the output of the previous iterations [13]. In this manner the Masked Autoregressive Flow (MAF) is trained, and the weights adjusted to transform samples from the base distribution, z , into samples from the target distribution, x , via a series of conditional probabilities, z_{n-1} .

Due to the invariance of the KL divergence and, similarly, the BMD under a change of variables, we can calculate their values in any transformed version of the original parameter space provided the prior and posterior undergo the same change of variables.

We can transform the target posterior samples, that we want our MAF to be able to replicate, into a Gaussian parameter space via the standard normal cumulative distribution function (CDF). This leads to an improvement in the accuracy of our density estimator because the target in this normalised space is a skewed and scaled version of z_0 .

Provided that we also transform the prior into the Gaussian space via the standard normal CDF, we can then use our density estimator to evaluate the log-probability densities and marginal Bayesian statistics. Generally, we can train a MAF to estimate the prior log-probability. However, in the case where the prior is uniform, or can be easily manipulated along with the posterior samples into a uniform parameter space, then the prior in the Gaussian space is the standard normal distribution, $\mathcal{N}(0, 1)$. MARGARINE assumes this is the case and that the posterior samples are taken from the uniform parameter space when calculating the marginal KL divergence and BMD, however, the true structure of the prior is not a limiting factor and the code can be easily manipulated to cope with more complex priors.

There are a number of tunable parameters involved when designing MAFs including the number of networks, the number of layers in each network, the number of epochs and the learning rate. All of these parameters can be explored using MARGARINE, and we use recommendations from a previous implementation [20].

3.2 Kernel Density Estimation

A simple 1D Kernel Density Estimator (KDE) is defined by

$$\mathcal{P}(x) = \frac{1}{nh} \sum_{i=1}^n K\left(\frac{x - x_i}{h}\right) \tag{7}$$

where h is known as the bandwidth, K is the kernel and n the number of samples in the set x . This scales into higher dimensions where x and x_i become n dimensional vectors and h becomes a 2D matrix of bandwidths. We use a multivariate Gaussian kernel where h is equivalent to the covariance matrix and x_i is equivalent to an n dimensional vector of means. Since the KDE is a sum of known

kernels with a known covariance matrix and set of means, then the probability distribution of the samples is trivially calculable, as is its logarithm.

We perform the same type of normalisation to the Gaussian space via a standard normal CDF, as is done when training MAFs, when generating our KDEs. We note that this transformation also allows the density estimator to better capture the edges of very flat and uniform posteriors.

Strictly speaking KDEs are not bijective transformations, but we can generate samples from them. This means that we can easily calculate the marginal statistics with a trained KDE, but transforming samples from the unit hypercube to the target density, when we want to use more complex priors in our nested sampling runs, is not so trivial (see section 3.5 in [21]).

Adapting a KDE to be bijective is a non-linear process and requires the use of a root-finding algorithm to transform from the hypercube to the KDE space. This is a slow process that is not currently optimized, but is fully implemented in MARGARINE. We note that the equivalent transformation using MAFs is much more computationally efficient.

There are fewer tunable parameters for the KDE, however we can change the bandwidth of the kernel. We use the Silverman [22] approach to calculate h but note that this can be modified with MARGARINE.

4 Application of KDEs and MAFs

4.1 Toy Example Posteriors

We illustrate the applications of the code using two different toy examples for which we know the KL divergence and BMD. We generate the examples using POLYCHORD and a Gaussian likelihood, both with five parameters, and these are shown in red in Fig. 1. The first has a series of correlations between the parameters (left-hand panel) and the second has a combination of uncorrelated parameters with both log-uniform and uniform priors on the parameters (right-hand panel).

We are able to use the samples from POLYCHORD and the analysis tool ANESTHETIC [23] to calculate the KL divergence and BMD for both sets of samples and these values are reported, with errors, in Fig. 1. We show a replica of the correlated samples using a KDE and uncorrelated samples using the MAF with values of \mathcal{D} and d listed for both types of density estimator.

The errors in \mathcal{D} and d are estimated by propagating both samples generated with the density estimator and the original samples through the density estimator to evaluate the log-probabilities and comparing the resultant statistics. If the density estimator is a perfect representation of the original posterior, then we would expect samples drawn from it to be from the same distribution as the original samples. This would lead to an approximate equivalence between the two log-probability distributions as functions of the associated nested sampling weights [24] and so any deviation we see gives us an indication of the error in our log-probability that can be propagated through to the marginal Bayesian statistics.

For the correlated samples, we see that the estimated KL divergence and BMD from the MAF are in close agreement with the ‘true’ value output from ANESTHETIC. The KDE estimate of the KL divergence is within one times its lower bound of the ‘true’ value, and the BMD estimate is also within one times its lower bound of the ANESTHETIC value. For the uncorrelated samples, again we see that the MAF KL divergence and BMD estimates are in agreement with the ANESTHETIC values. For the KDE, the KL divergence is within two times its lower bound of the ANESTHETIC value. The BMD is within one times its upper bound of the ‘true’ value, however, we note that there is a large uncertainty on this result. Typically, the upper and lower bounded range on the BMD estimates are larger than for the KL divergence estimates because it has a more complex dependence on $\log \mathcal{L}$. Future work is needed to investigate whether improvements can be made to the BMD estimates by modifying the MAF loss function, network configurations or KDE bandwidths among other tunable parameters.

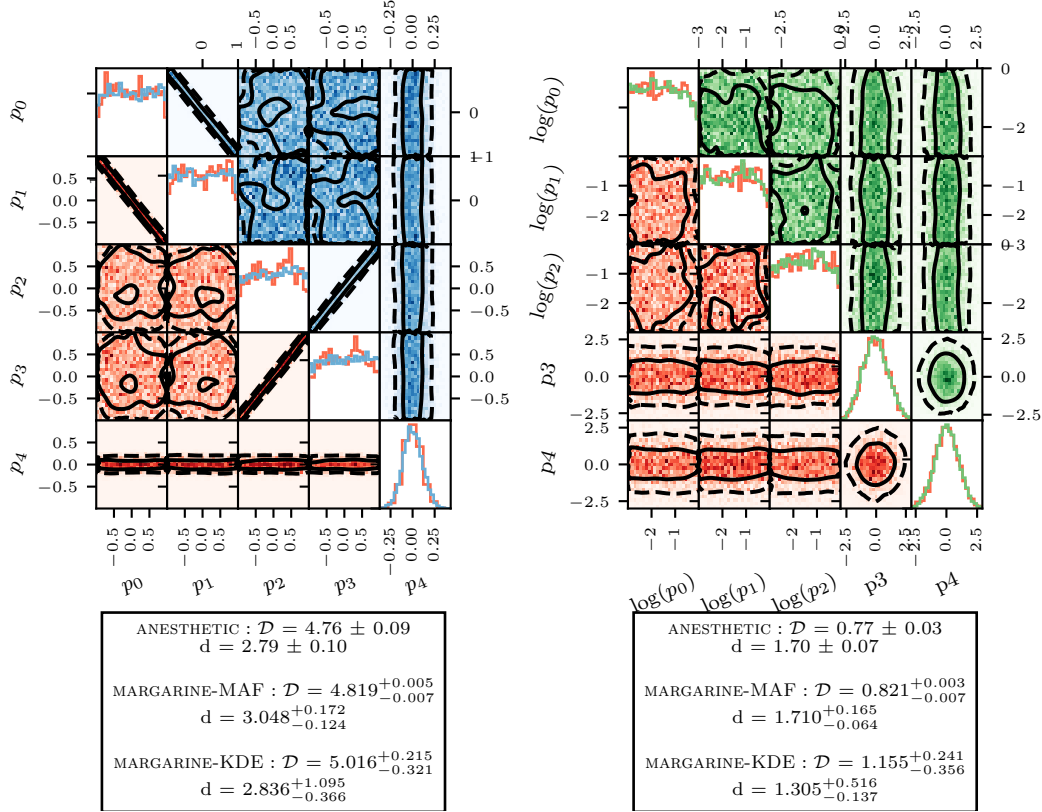


Figure 1: **Left Panel:** The graph shows a set of correlated nested samples from POLYCHORD in red along with a reconstruction from a trained KDE. Listed are the corresponding ‘true’ values for the KL divergence and BMD from ANESTHETIC and the estimated values from MARGARINE using both a KDE and MAF. **Right Panel:** An equivalent graph for a set of uncorrelated samples with both log-uniform and uniform priors on the parameters, shown in red. The green samples are taken from a trained MAF, and we report the ‘true’ Bayesian statistics values along with estimates calculated using a MAF and KDE with MARGARINE.

4.2 Cosmological Example Posteriors

4.2.1 Radio Experiment for the Analysis of Cosmic Hydrogen

The Radio Experiment for the Analysis of Cosmic Hydrogen (REACH) is an experiment aiming to detect the sky-averaged (global) 21-cm signal in the frequency range 50 – 170 MHz. The global 21-cm signal is the differential brightness temperature between the radio background, T_r and the spin temperature, T_s , of neutral hydrogen during the Cosmic Dawn and Epoch of Reionization. T_s quantifies the ratio of the number of neutral hydrogen atoms with proton and electron spins aligned versus anti-aligned.

The signal manifests itself as an absorption trough when the first stars begin to form in the early universe, and Lyman- α coupling drives the spin temperature down to the gas kinetic temperature. Various heating mechanisms then begin, particularly as the first X-ray sources form, and the spin temperature is raised back up to and sometimes in excess of the radio background. UV emission then begins to ionize the neutral hydrogen and the signal vanishes during the Epoch of Reionization. The global 21-cm signal is predicted to be of order 100 mK in magnitude and is masked by foregrounds from our own Galaxy [25], extragalactic radio sources [26] and the ionosphere [27] which collectively are 4-5 orders of magnitude brighter than the signal. To a crude approximation, the signal can be modelled with a Gaussian absorption profile.

The REACH data analysis pipeline uses nested sampling, implemented with POLYCHORD, to model the foregrounds, chromatic effects of the beam and the global 21-cm signal in the data. The pipeline

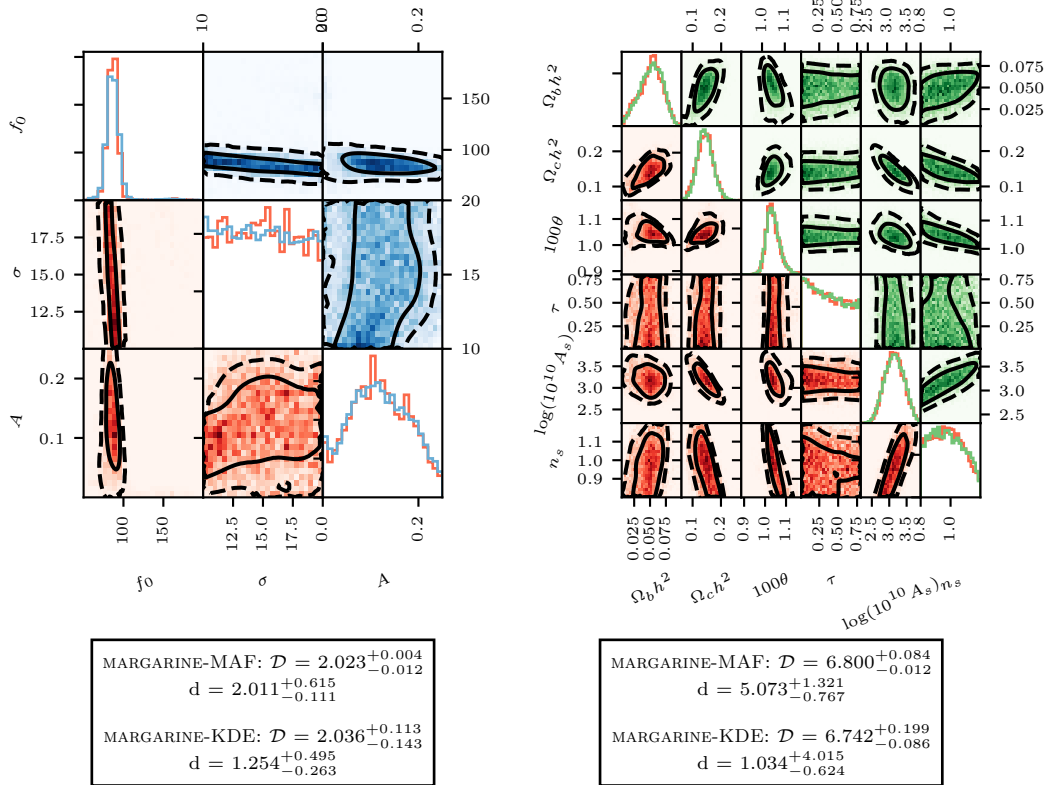


Figure 2: **Left Panel:** The signal subspace, in red, from a simulated observation and analysis with the REACH 21-cm experiment along with samples, in blue, from KDE trained on the three signal parameters effectively marginalising over the other thirteen parameters in the fit. We report the marginal KL divergence and BMD found for this set of three parameters using both a MAF and KDE. **Right Panel:** The cosmological subspace for the year one DES samples shown in red, along with a set of samples taken from a trained MAF in green. Again, we report the corresponding marginal Bayesian statistics calculated with MARGARINE.

has been extensively tested on mock observations [12, 28, 29, 30, 31] and we demonstrate the application of MARGARINE to an example set of samples from the pipeline. Where we have generated mock observational data using an all-sky map and injected a Gaussian signal profile with an amplitude of $A = 155$ mK, a central frequency of $f_0 = 85$ MHz and a standard deviation of $\sigma = 15$ MHz.

The samples correspond to a single snapshot observation taken from the Karoo radio observatory with a dipole antenna and modelled with a foreground model that takes advantage of the spectral structure of the sky, a chromaticity correction, Gaussian noise and a Gaussian signal profile corresponding to a 16 dimensional parameter space. In the left-hand panel of Fig. 2 we show the signal parameter samples in red, having marginalised over the other 13 parameters, and the corresponding KDE reconstruction from MARGARINE in blue. We see a reasonable consistency between the marginal KL divergence calculated for these samples when using both types of density estimator built into MARGARINE.

However, we note that there are some differences in the BMD estimate with the MAF giving a larger value for dr . From a visual inspection of the samples we would expect the BMD to be around 1-2 due to the tight constraint on f_0 and weaker but still non-trivial constraint on A meaning that both estimates are consistent with expectations and each other within $\lesssim 3$ times their respective bounds.

4.2.2 Dark Energy Survey

The Dark Energy Survey (DES) is designed to help us understand why the Universe’s rate of expansion is accelerating. The goal of the collaboration is to map millions of galaxies, thousands of supernova

and large scale cosmic structures in order to help understand the dark energy which makes up 70% of the universe. Specifically, the survey has targeted the measurements of the dark matter and dark energy densities as well as the dark energy equation of state [32] by investigating galaxy clustering, gravitational lensing and supernova distances.

We use samples from the Year 1 DES analysis [33] which aimed to constrain the baryon density parameter, Ω_b , the dark matter density parameter, Ω_c , the approximate ratio of the sound horizon to the angular diameter distance, θ , the optical depth of the CMB to reionization, τ and the amplitude and tilt of the power spectrum, A_s and n_s . We note that the Year 3 DES results have been published [6, 5] but that the samples have not been made publicly available. The Year 1 samples from the cosmological subspace are shown in red in the right-hand panel of Fig. 2, where we have marginalised over the 20 nuisance parameters, along with a MAF reconstruction of the subspace in green.

Unlike the toy examples and REACH samples, the DES cosmological samples do not have uniform priors and cannot easily be transformed into a space in which the priors are uniform. As a result, we have to use the density estimators built into MARGARINE to evaluate both the log-probability of the posterior and the prior if we want to calculate marginal statistics.

While this is possible it is expected to lead to an increased uncertainty in the marginal statistics, for example this can be seen for the marginal BMD values reported in Fig. 2. The problem is further complicated by the size of the cosmological parameter space, we expect larger parameter spaces to be harder to replicate well with MARGARINE. We find that both methods with the two different density estimates give consistent marginal KL divergences.

Again the density estimators give us different estimates for the BMD however they can be considered consistent due to the large error bars, and consistent with expectations from a visual examination of the graph which suggests the BMD should be between ≈ 3 and ≈ 4 .

5 Conclusions

In this paper we have demonstrated the application of two different types of density estimator, Masked Autoregressive Flows and Kernel Density Estimators, to the calculation of marginal Bayesian statistics. The evaluation of marginal KL divergences and Bayesian Model Dimensionalities will allow for improved comparison of the constraining power of different experiments targeting the same astrophysical or cosmological signals with different systematics or nuisance parameters. In turn, this can lead to improvements in experimental design with techniques that provide more information about the signals of interest being pursued in the future.

We illustrate the principle of marginal Bayesian statistics with some toy examples in which we know the ‘true’ values of the KL divergence and BMD and some real world examples. It is shown that the code can recover reasonable estimates of the statistics for the toy examples and provide sensible answers for the cosmological samples.

MARGARINE has already been used in several works, including [31] and two in prep papers on the effects of modelling data in time separate bins in the REACH pipeline and an analysis of the data from the global 21-cm experiment SARAS3. The applications of the code have been further explored in [34].

Acknowledgments and Disclosure of Funding

HTJB acknowledges the support of the Science and Technology Facilities Council (STFC) through grant number ST/T505997/1. WJH and AF were supported by Royal Society University Research Fellowships. PHS acknowledges support from a McGill Space Institute Fellowship and the Canada 150 Research Chairs Program. EdLA was supported by the STFC through the Ernest Rutherford Fellowship. JA was supported by the research project grant “Fundamental Physics from Cosmological Surveys” funded by the Swedish Research Council (VR) under Dnr 2017-04212.

References

- [1] Kullback, S., R. A. Leibler. On Information and Sufficiency. *The Annals of Mathematical Statistics*, 22(1):79–86, 1951. Publisher: Institute of Mathematical Statistics.

- [2] Handley, W., P. Lemos. Quantifying dimensionality: Bayesian cosmological model complexities. *Phys. Rev. D*, 100(2):023512, 2019.
- [3] Planck Collaboration, N. Aghanim, Y. Akrami, et al. Planck 2018 results. VI. Cosmological parameters. *A&A*, 641:A6, 2020.
- [4] Abbott, T. M. C., F. B. Abdalla, A. Alarcon, et al. Dark Energy Survey year 1 results: Cosmological constraints from galaxy clustering and weak lensing. *Phys. Rev. D*, 98(4):043526, 2018.
- [5] Friedrich, O., F. Andrade-Oliveira, H. Camacho, et al. Dark Energy Survey year 3 results: covariance modelling and its impact on parameter estimation and quality of fit. *MNRAS*, 508(3):3125–3165, 2021.
- [6] Abbott, T. M. C., M. Aguena, A. Alarcon, et al. Dark Energy Survey Year 3 results: Cosmological constraints from galaxy clustering and weak lensing. *Phys. Rev. D*, 105(2):023520, 2022.
- [7] The HERA Collaboration, Z. Abdurashidova, J. E. Aguirre, et al. HERA Phase I Limits on the Cosmic 21-cm Signal: Constraints on Astrophysics and Cosmology During the Epoch of Reionization. *arXiv e-prints*, arXiv:2108.07282, 2021.
- [8] Ghara, R., S. K. Giri, G. Mellema, et al. Constraining the intergalactic medium at $z \approx 9.1$ using LOFAR Epoch of Reionization observations. *Monthly Notices of the Royal Astronomical Society*, 493(4):4728–4747, 2020.
- [9] Mondal, R., A. Fialkov, C. Fling, et al. Tight constraints on the excess radio background at $z = 9.1$ from LOFAR. *MNRAS*, 498(3):4178–4191, 2020.
- [10] Greig, B., C. M. Trott, N. Barry, et al. Exploring reionization and high- z galaxy observables with recent multiredshift MWA upper limits on the 21-cm signal. *Monthly Notices of the Royal Astronomical Society*, 500(4):5322–5335, 2020.
- [11] Ghara, R., S. K. Giri, B. Ciardi, et al. Constraining the state of the intergalactic medium during the epoch of reionization using MWA 21-cm signal observations. *Monthly Notices of the Royal Astronomical Society*, 2021. Stab776.
- [12] Anstey, D., E. d. L. Acedo, W. Handley. A General Bayesian Framework for Foreground Modelling and Chromaticity Correction for Global 21cm Experiments. *arXiv:2010.09644 [astro-ph]*, 2020. ArXiv: 2010.09644.
- [13] Papamakarios, G., T. Pavlakou, I. Murray. Masked Autoregressive Flow for Density Estimation. *arXiv e-prints*, arXiv:1705.07057, 2017.
- [14] Rosenblatt, M. Remarks on Some Nonparametric Estimates of a Density Function. *The Annals of Mathematical Statistics*, 27(3):832–837, 1956. Publisher: Institute of Mathematical Statistics.
- [15] Parzen, E. On Estimation of a Probability Density Function and Mode. *The Annals of Mathematical Statistics*, 33(3):1065–1076, 1962. Publisher: Institute of Mathematical Statistics.
- [16] Skilling, J. Nested Sampling. *AIP Conference Proceedings*, 735(1):395–405, 2004. _eprint: <https://aip.scitation.org/doi/pdf/10.1063/1.1835238>.
- [17] Handley, W., P. Lemos. Quantifying tensions in cosmological parameters: Interpreting the DES evidence ratio. *Phys. Rev. D*, 100(4):043504, 2019.
- [18] Glanville, A., C. Howlett, T. M. Davis. Full-Shape Galaxy Power Spectra and the Curvature Tension. *arXiv e-prints*, arXiv:2205.05892, 2022.
- [19] Kingma, D. P., P. Dhariwal. Glow: Generative Flow with Invertible 1x1 Convolutions. *arXiv e-prints*, arXiv:1807.03039, 2018.
- [20] Alsing, J., W. Handley. Nested sampling with any prior you like. *MNRAS*, 505(1):L95–L99, 2021.
- [21] Handley, W. J., M. P. Hobson, A. N. Lasenby. POLYCHORD: next-generation nested sampling. *MNRAS*, 453(4):4384–4398, 2015.
- [22] Silverman, B. W. *Density estimation for statistics and data analysis*. Routledge, 2018.
- [23] Handley, W. anesthetic: nested sampling visualisation. *The Journal of Open Source Software*, 4(37):1414, 2019.
- [24] Harrison, D., D. Sutton, P. Carvalho, et al. Validation of Bayesian posterior distributions using a multidimensional Kolmogorov-Smirnov test. *MNRAS*, 451(3):2610–2624, 2015.
- [25] Bernardi, G., A. G. de Bruyn, M. A. Brentjens, et al. Foregrounds for observations of the cosmological 21 cm line. I. First Westerbork measurements of Galactic emission at 150 MHz in a low latitude field. *A&A*, 500(3):965–979, 2009.
- [26] Niřu, I. C., H. T. J. Bevins, J. D. Bray, et al. An updated estimate of the cosmic radio background and implications for ultra-high-energy photon propagation. *Astroparticle Physics*, 126:102532, 2021.

- [27] Shen, E., D. Anstey, E. de Lera Acedo, et al. Quantifying ionospheric effects on global 21-cm observations. *MNRAS*, 503(1):344–353, 2021.
- [28] Anstey, D., J. Cumner, E. de Lera Acedo, et al. Informing antenna design for sky-averaged 21-cm experiments using a simulated Bayesian data analysis pipeline. *MNRAS*, 509(4):4679–4693, 2022.
- [29] Cumner, J., E. De Lera Acedo, D. I. L. de Villiers, et al. Radio antenna design for sky-averaged 21 cm cosmology experiments: the REACH case. *arXiv e-prints*, arXiv:2109.10098, 2021.
- [30] Scheutwinkel, K. H., W. Handley, E. de Lera Acedo. Bayesian evidence-driven likelihood selection for sky-averaged 21-cm signal extraction. *arXiv e-prints*, arXiv:2204.04491, 2022.
- [31] Scheutwinkel, K. H., E. de Lera Acedo, W. Handley. Bayesian evidence-driven diagnosis of instrumental systematics for sky-averaged 21-cm cosmology experiments. *arXiv e-prints*, arXiv:2204.04445, 2022.
- [32] The Dark Energy Survey Collaboration. The Dark Energy Survey. *arXiv e-prints*, astro-ph/0510346, 2005.
- [33] Handley, W., P. Lemos. Quantifying tensions in cosmological parameters: Interpreting the DES evidence ratio (supplementary inference products). *Zenodo*, 2020.
- [34] Bevins, H., W. Handley, P. Lemos, et al. Marginal Bayesian Statistics Using Masked Autoregressive Flows and Kernel Density Estimators with Examples in Cosmology. *arXiv e-prints*, arXiv:2207.11457, 2022.